Available online at www.sciencedirect.com

ScienceDirect

journal homepage: www.elsevier.com/locate/issn/15375110

Research Paper

A novel image processing algorithm to separate linearly clustered kiwifruits

Longsheng Fu [a,b,c,d], Elkamil Tola [e], Ahmad Al-Mallahi [f], Rui Li [a], Yongjie Cui [a,b,c,*]

[a] College of Mechanical and Electronic Engineering, Northwest A&F University, Yangling, 712100, China
[b] Key Laboratory of Agricultural Internet of Things, Ministry of Agriculture and Rural Affairs, Yangling, Shaanxi, 712100, China
[c] Shaanxi Key Laboratory of Agricultural Information Perception and Intelligent Service, Yangling, Shaanxi, 712100, China
[d] Center for Precision and Automated Agricultural Systems, Washington State University, Prosser, WA, 99350, USA
[e] Precision Agriculture Research Chair, King Saud University, Riyadh, 11451, Saudi Arabia
[f] Department of Engineering, Faculty of Agriculture, Dalhousie University, Truro, Nova Scotia, B2N 5E3, Canada

ARTICLE INFO

Article history:
Received 13 April 2018
Received in revised form
5 April 2019
Accepted 30 April 2019
Published online 21 May 2019

Keywords:
Machine vision
Segmentation
Detection
Calyx
Counting

This research work aims at developing a machine vision system capable of distinguishing kiwifruits on plants prior to harvest. The methodology was based on developing an algorithm able to detect each fruit, even when they are clustered in a line. It segments the fruits from the background, counts the number of fruits in each cluster, and identifies the edges of each fruit. After segmentation, the algorithm initially distinguishes between the fruit skin and calyx based on colour differences using selected hue and red channels. Next, a calyx line is drawn to connect all the calyxes in one cluster together. Then, the periphery of each cluster is scanned to find the contact points between the adjacent fruits. Finally, a separating line is drawn between the two closest contact points, provided that this line intersected almost vertically the calyx line. The separating lines determine the borders of each fruit and enable singling them out. The results showed that 93.7% of the fruit calyxes were correctly detected. In night-time with flash, 92.0% of the fruits were separated and counted correctly by the algorithm.

© 2019 IAgrE. Published by Elsevier Ltd. All rights reserved.

1. Introduction

China is the largest country producing kiwifruits worldwide, with a yield of 2.4 Mt in 2016 from a cultivated area of 197,048 ha (UN Food & Agriculture Organization, 2018). The Shaanxi Province has the largest production, accounting for approximately 70% and 33% of the local and global production, respectively (Hu et al., 2017). Harvesting kiwifruits in this area mainly depends on manual picking, which is labour-intensive (Fu, Sun, Li, & Wang, 2016). Therefore, introducing mechanical harvesting is highly desired.

* *Corresponding author*. College of Mechanical and Electronic Engineering, Northwest A&F University, Yangling, 712100, China.
E-mail address: cuiyongjie@nwsuaf.edu.cn (Y. Cui).
https://doi.org/10.1016/j.biosystemseng.2019.04.024
1537-5110/© 2019 IAgrE. Published by Elsevier Ltd. All rights reserved.

Nomenclature

L*a*b*	a colour space, L* for the lightness and a* and b* for the green–red and blue–yellow colour components
RGB	a colour space, R for red colour component, G for green colour component, and B for blue colour component
HSV	a colour space, H for hue colour components, S for saturation colour components, and V for value colour components
P	program
PCA	principal component analysis
PCs	principal components
A_i	a column for each colour channel
A_i'	mean of each column
A_i''	variance of each column
A_o	normalised matrix
A_{co}	covariance matrix of A_o
λ	eigenvalues of A_{co}
W	eigenvectors of A_{co}
k	number of labelled black areas
fn	fruit number in a cluster
m_j	number of pixels in the j^{th} labelled black area
X_j	an array to store the positions in width of the pixels of the j^{th} labelled black area
Y_j	an array to store the positions in height of the pixels of the j^{th} labelled black area
x_{cj}	mean position in width of the j^{th} labelled black area
y_{cj}	mean position in height of the j^{th} labelled black area
p_s	number of fruit pixels inside the circular mask
r	radius of the circular mask
c_s	concaveness value
p_i	concavity point
l_i	distance between the nearest two detected calyxes
l	sum of all l_i

Kiwifruits are commercially grown on sturdy support structures such as T-bars and pergolas (Huang & Ferguson, 2001). The T-bar trellis is common in China because of its low cost (Lu et al., 2016). It consists of a 1.7 m high post and an approximately 1.7 m wide cross arm, which may have slightly different widths depending on the orchard geometry. Wires run on the top of the cross arms and connect them to each other from the middle and on both sides. The upper stems of the kiwi plants are tied to the top wires, so that the egg-sized kiwifruits are hanging downwards, making them easy to pick during the harvest season (Fu, Zhang, et al., 2015; Mu et al., 2017; Mu, Liu, Cui, Fu, & Gejima, 2018). This workspace is more structured in comparison to other fruit trees, and therefore, it is easier to perform mechanical work.

Machine vision is widely used to detect fruits for harvesting robots (Bechar & Vigneault, 2016). Detection algorithms have been developed for apples (Lv, Zhao, Ji, & Ding, 2016; Si, Liu, & Feng, 2015; Silwal et al., 2017), citrus fruits (Mehta & Burks, 2014; Okamoto & Lee, 2009) tomatoes (Yamamoto, Guo, & Ninomiya, 2016). University of Florida applied machine vision to recognise oranges by detecting the fruit colour and shape (Hannan, Burks, & Bulanon, 2009), etc. Also, researchers in Washington State University proposed an image processing method consisting of a circular Hough transform to clearly identify visible fruits, and a blob analysis to detect partially visible apples as a concept of hierarchical fruit identification (Silwal et al., 2017; Silwal, Karkee, & Zhang, 2016). In general, these studies have achieved fruit identification accuracy ranging from 80% to 95% and have reported that varying lighting conditions, clustering, and occlusion are the most significant challenges to accurately identify fruits in orchards.

Researches on kiwifruits recognition are being conducted in China and New Zealand, in particular, as the two main countries producing this fruit. Cui et al. (2013) studied fruit recognition and feature extraction methods based on the colour and shape characteristics of the kiwifruits on trees with daytime lighting. Zhan, He, and Shi (2013) developed an image processing technique for segmenting kiwifruits from the background based on the Adaboost algorithm. Su, Fu, Zhang, and Cui (2013) employed 0.9R-G colour component to extract the characteristic parameters of kiwifruits using the Canny operator for edge detection and the ellipse Hough transformation for fruit recognition. These researches addressed the daytime harvesting scenario under sunlight and captured kiwifruit images by placing the camera near the underside of the canopy with its central axis approximately parallel to the canopy. However, this causes the background of the image to contain pendulous foliage or distant non-target fruits, which can add excessive noise at image segmentation, which affect the accuracy. Moreover, since kiwifruits grow in clusters, the target fruits may overlap in the images. This will also lead to difficulties in recognising each target fruit and reduce the recognition accuracy.

Another image capturing method of kiwifruits is to place the camera underneath the fruits, so that its central axis would be perpendicular to the canopy (Fu, Wang, et al., 2015; Scarfe, Flemmer, Bakker, & Flemmer, 2009). When viewed from the bottom, the target fruits and their calyxes (each fruit has one calyx) can be included in the field of view of the camera, and the fruits would be adjacent to each other rather than overlapping (Fig. 1). Scarfe (2012) segmented a bottom viewed kiwifruit image by subtracting a predefined reference colour range and used the Sobel filter to detect the fruit and the calyx edges. He, then, utilised a circular template with a 28-pixel diameter to scan the extracted calyx area and assigned the centre of mass as the position of each fruit. His algorithm could positively identify 83.6% of the kiwifruits with single-frame processing time ranging from 15.2 to 28.7 s. Fu et al. (2017) segmented a bottom viewed kiwifruit image using Otsu threshold in 1.1R-G and eliminated the noises through a morphological operation and area thresholding. They, then, extracted the fruits boundaries using a Canny filter. Finally, they employed a minimal bounding rectangle and an elliptical Hough transform to detect each target fruit area. Their algorithm achieved a recognition rate of 88.3% in an average time period of 0.83 s to segment one image and

Fig. 1 – Kiwifruits from bottom view in (a) single, (b) linear cluster, (c) other cluster.

1.51 s to detect each fruit. The former algorithm mainly used the colour and shape of the calyx, while, the latter employed the colour and shape of the fruit. In general, the success rate and processing time of robotic harvesting of kiwifruits have been lower than that of other fruits, such as apple and oranges. Therefore, it was necessary to develop a fast algorithm to detect kiwifruits at high success rates using both colour and shape of the fruit and calyx.

According to a field survey in Shaanxi province (Fu, Wang, et al., 2015), most kiwifruits are grouped together and were defined as linear clusters, 87.3% of which only have two adjacent fruits (Fig. 1b), while the remaining clusters have three or more adjacent fruits (Fig. 1c). If the linear cluster could be detected at a high success rate, this means that at least 87.3% of kiwifruits can be successfully detected. Therefore, this study, which focused on the linear cluster, is not limited to only detect the linear cluster with the centre of each kiwifruit, but also separate them accurately. Some researches were conducted to split touching objects, such as kernels, and achieved good results (Mebatsion & Paliwal, 2011; Zhong, Ping, Yao, & Mao, 2010). However, these researches dealt with digital images with controlled simple and consistent backgrounds, which are much different from the outside field condition.

Incidentally, taking the images at night-time could overcome the problem of low work efficiency and help in reducing fruit damage because the fruit temperature is lower than that during the daytime. In addition, artificial lights can be used while capturing images, to ensure constant illumination instead of ambient light. Therefore, the objective of this study was to develop an image processing algorithm to detect and separate linear clustered kiwifruits at a high success rate during both day and night time. It also aimed to detect each individual fruit when they were clustered in-line by identifying the fruit calyx and contact points between the adjacent fruits.

2. Materials and methods

2.1. Image capturing

The method of capturing images used in this study was based on placing the camera underneath the fruits, with its central axis perpendicular to the canopy. A very common single-lens reflex camera (Canon S110, Canon Inc., Tokyo, Japan) on "P" mode with a resolution of 640 × 360, was utilised for this study. The camera was placed at around 20 cm underneath the fruits, so that one cluster of kiwifruits could be included in the field of view of the camera. RGB (Red, Green, and Blue) images of the fruits were taken during three harvest seasons (2014, 2015 and 2016) of the most common 'Hayward' cultivar at the Meixian Kiwifruit Experimental Station (34°07′39″N, 107°59′50″E, and 648 m in altitude), Northwest A&F University, Shaanxi, China.

A total of 24 linear clusters including 99 fruits (the number of fruits contained in one cluster varied between 2 and 7) were selected as a calibration dataset to develop the algorithm. On the other hand, 150 linear clusters including 487 fruits were captured as a validation dataset to test the algorithm. The distribution of the clusters during the three harvest seasons is given in Table 1. Three images were captured for each cluster under different periods of time and lighting conditions (daytime without flash, daytime with flash, and night time with flash), as shown in Fig. 2. To facilitate the analysis of data, the clusters were divided, according to the number of fruits in the cluster, into four categories (2-Fruit, 3-Fruit, 4-Fruit and 4+-Fruit clusters).

2.2. Fruit area segmentation

The noticeable features of the bottom view images (Figs. 1, 2 and 3a) include colour differences from the background, brown calyx remnants at the lower end of the fruit, reflective bright arc around the blossom, end and distinguishable borders around the calyx, often at the edge of the fruits. Therefore, the image processing algorithm was developed to detect each target kiwifruit based on the colour and shape of fruit and calyx.

The colour of the fruits was first exploited to remove unwanted scene information. Because of the expected

Table 1 – Distribution of the clusters and kiwifruits during the three harvest seasons.

	Image Capturing date	Number of clusters	Number of fruits
Calibration Dataset	October 23, 2014	8	33
	November 04, 2015	8	34
	October 19, 2016	8	32
	Total	**24**	**99**
Validation Dataset	October 23, 2014	50	163
	November 04, 2015	50	163
	October 19, 2016	50	161
	Total	**150**	**487**

Fig. 2 – Linear clusters of kiwifruits under different periods of time and lighting conditions: (a) daytime without flash, (b) day time with flash and (c) night time with flash.

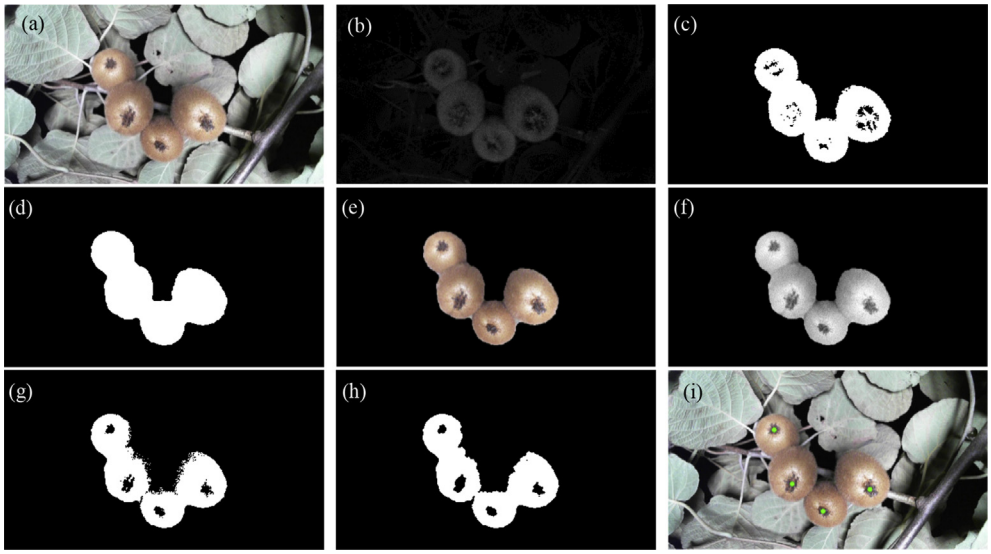

Fig. 3 – The process of detecting calyxes. (a) Original RGB kiwifruit image, (b) Grey image of the 1.1R-G, (c) Segmented image by Otsu threshold in the 1.1R-G, (d) Largest area of fruits after eliminating noise using morphological process and removing smaller areas, (e) Fruits area image, (f) Selected grey image of the area of fruits, (g) Segmented image of skin and calyx by Otsu threshold, (h) Opened image for detecting calyxes, (i) Detected calyxes (green dots) on the original kiwifruit images.

improvement in the segmentation results after integrating the *n*R-G coefficient (Fu, Wang, et al., 2015), the 1.1R-G model was selected for image segmentation in this study (Fig. 3b). The threshold which divides the grey image pixels into two classes was determined using the Otsu method (Otsu, 1975), the result is shown in Fig. 3c. Next, a morphological operation was applied to remove noise that adheres to the target fruits, such as branches, whereas area thresholding was employed to eliminate the remaining small noise areas. Figure 3d shows the noise-free fruit image, which was multiplied by the original RGB image (Fig. 3a) to obtain the fruits area in white as shown in Fig. 3e.

2.3. *Detection of the calyxes*

Sample pixels of fruit skin and calyx were taken from the fruit area image in the calibration dataset to study their colour differences for segmentation. The pixels were collected using an original sampling program written in MATLAB 2016a (Mathworks, 2016), able to display an RGB colour image directly. After each image was displayed, 10 pixels of each fruit skin were selected first by random clicking, followed by 10 pixels of each calyx. In order to avoid sampling the same pixel, a red mark appeared on the selected pixels while the colour information was recorded in a data file. A total of 2970 pixels of fruit skin and calyx were collected. Another colour space HSV (Hue, Saturation and Value) in the range of [0, 1] was obtained from the RGB colour values of each pixel using the MATLAB function 'rgb2hsv'. The advantage of the HSV is that each of its attributes corresponds directly to the basic colour concepts, making it conceptually simple. Therefore, this work was inspired by the fact that the HSV is more in tune with the human colour perception (Sobottka & Pitas, 1996). In addition, the HSV colour space is robust to the illumination variation as the Hue (H) describes a pure colour (Chaves-González, Vega-Rodríguez, Gómez-Pulido, & Sánchez-Pérez, 2010). Thus, 6 colour channels (Red, Green, Blue, Hue, Saturation and Value) were investigated for segmenting the pixels between fruit skin and calyx.

Principal component analysis (available in MATLAB as the 'pca' function) was used to select the significant colour channels between the skin and calyx. Each colour channel was converted into a column A_i, and normalised in the resulting matrix $A = [A_1, A_2, \ldots, A_6]^n$, where n is the 5940 sampled pixels of the skin and calyx, using Equation (1):

$$A_{io} = \left(A_i - A_i^{'}\right)/A_i^{''} \quad (1)$$

where A_i ($i = 1, 2, \ldots, 6$) is the index of the original Red, Green, Blue, Hue, Saturation and Value channels, respectively; A_i' and A_i'' are the mean and variance of each channel, respectively; and A_{io} represents the normalised channel. The normalised matrix $A_o = [A_{1o}, A_{2o}, \ldots, A_{6o}]^n$ was consequently obtained.

The covariance matrix A_{co} of A_o was calculated as using Equation (2). It can be decomposed into its corresponding eigenvalues and eigenvectors, as shown in Equation (3).

$$A_{co} = \sum_{j=1}^{N} A_o A_o^T \quad (2)$$

$$A_{co} = \lambda W \quad (3)$$

where $\lambda = \text{diag}(\lambda_1, \lambda_2, \ldots, \lambda_6)$ and $W = [w_1, w_2, \ldots, w_6]$. λ_i ($i = 1, 2, \ldots, 6$) and w_i ($i = 1, 2, \ldots, 6$) are the eigenvalues and eigenvectors of the A_{co}, respectively.

Instead of using the principal components (PCs) directly, the original first two channels that contribute most to the PCs were selected. Then, Linear Discriminant Analysis was applied to obtain a classification formula for segmenting the pixels into skin and calyx using the MATLAB function 'fitcdiscr' on the two selected channels.

Once the skin and calyx pixels (Fig. 3e) were classified using the classification formula (Fig. 3g), the morphological process was again applied to remove the noise and connect the pixels of each calyx area (Fig. 3h). The black areas, including the calyx areas and the background, were labelled and sorted by the number of pixels from m_1 to m_k (k is the number of the labelled black areas); and their pixel positions (X_j, Y_j) ($j = 1, 2, \ldots, k$) were stored in an array.

The largest black area m_1 is the background, and the second largest black area m_2 is the calyx area which is used as the reference area. Since the calyx areas differ in a small range in a single image, the calyx areas were judged compared to the reference area m_2. If a black area m_j ($2 < j \leq k$) in the image was smaller than the reference area m_2 and, simultaneously, larger than 1/5 of the reference area m_2, then it is a calyx area. This comparison was looped until m_j ($2 < j \leq k$) is less than 1/5 of the reference area m_2 for the first time. Accordingly, the number of calyx areas was determined, meaning that the number of fruits in a cluster is $fn = j - 2$. Next, the mean position (x_c, y_c) of each calyx area was calculated using Equation (4) as the centre of each fruit, as shown in Fig. 3i.

$$x_{cj} = \frac{\sum_1^{m_j} x}{m_j}, y_{cj} = \frac{\sum_1^{m_j} y}{m_j} \quad (4)$$

where (x_{cj}, y_{cj}) is the mean position of the j^{th} ($j = 2, \ldots, fn+1$) labelled black area, and m_j is the number of pixels in the j^{th} labelled black area.

2.4. Fruit separation

Since kiwifruits are convex, an obvious feature of adjacent fruits is the presence of concavities in their position. Therefore, the adjacent fruits can be separated by checking for concave shapes. In this paper, a method based on a circular mask was modified to detect the concavity point. The centre of the circular mask is on the contour of the fruit area (Fig. 3d); and the radius of the circular mask, which can be adapted to the size of fruit, was set to five pixels for kiwifruits, and notated by r, as shown in Fig. 4a. Every point of the contour has a concaveness value c_s expressed as in Equation (5).

$$c_s = p_s/\pi r^2 \quad (5)$$

where πr^2 is the pixel area of the circular mask which is 79 in this study, s runs over the contour started from the left top pixels and p_s is the number of fruit pixels inside the circular mask, as shown in Fig. 4a.

When the circular mask was used to determine the concaveness, a series of concaveness was found along the boundary of the binary image of adjacent fruits, but there was a local maximum value when s runs above the concave point, as shown in Fig. 4b. The local maximum values which are greater than 0.5 were extracted as candidate concavity points.

Unlike the researches that utilised the concavity point to separate adjacent objects in digital images with a controlled sample and consistent background (Mebatsion & Paliwal, 2011; Zhong et al., 2010), the background of kiwifruit image is outdoors and under uncontrolled conditions. This makes it more difficult to segment the kiwifruits from the background accurately at the boundaries of the fruits which will have more local maximum values of concaveness. Figure 5b shows the concaveness along the boundary of adjacent kiwifruits presented in the Fig. 5a. There are nine local maximum values greater than 0.5 and were detected as concavity points from Fig. 5c. However, there are only six actual concavity points (p_2, p_4, p_5, p_7, p_8 and p_9) marked as red square dots in Fig. 5b.

Lastly, a new method to separate the fruits, based on the positions of the detected candidate concavity points and the calyxes, was developed and added to the algorithm to separate the kiwifruits which is consisted of the following 6 steps:

- Step 1: Selecting the first two calyxes by scanning the image from top to bottom and from left to right.
- Step 2: Calculating the distances of all the detected concavity points to the first two calyxes.
- Step 3: Selecting the first two concavity points closest to the first two calyxes, and checking if their line crosses the line between the two calyxes with an angle close to 90°. If the lines intersect, the two concavity points will be positively identified and their line is the correct splitting path and Step 4 is skipped.
- Step 4: Selecting the next closest concavity point to perform the same step as the first closest concavity point or second closest concavity point until the lines intersect.
- Step 5: Removing the left-top fruit and its concavity points.
- Step 6: Repeating the Step 5 until all the calyxes are separated.

The flow chart of this method is shown in Fig. 6, and the result of applying it on Fig. 2 is shown in Fig. 7. The proposed algorithm was developed in MATLAB 2016a on a laptop ThinkPad T400 2.53 GHz CPU (Core 2 Duo P8700) and 4 GB RAM.

3. Results and discussions

3.1. Segmentation between fruit skin and calyx

Figure 8 shows the distribution of the Red, Green, Blue, Hue, Saturation and Value channels of the 5940 skin and calyx pixels sampled from the calibration dataset. The Red, Green

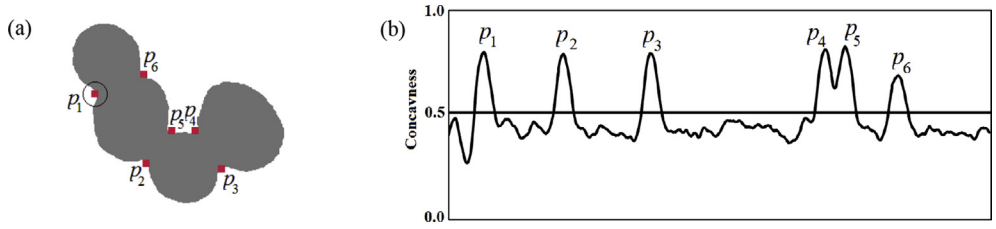

Fig. 4 – (a) Concavity points (red square dots) based on a circular mask; (b) Concaveness along the boundary of adjacent kiwifruits (the curve has been smoothed). (For interpretation of the references to colour in this figure legend, the reader is referred to the Web version of this article.)

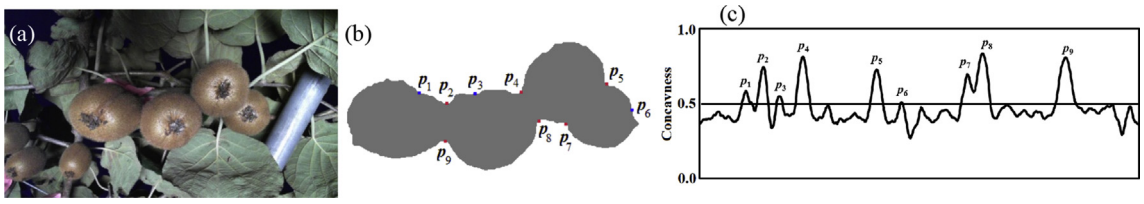

Fig. 5 – (a) RGB kiwifruit image; (b) Detected concavity points (red square dots are positively identified, and blue square dots are false positive) of Fig. 5a; (c) Concaveness along the boundary of adjacent kiwifruits in Fig. 5b.

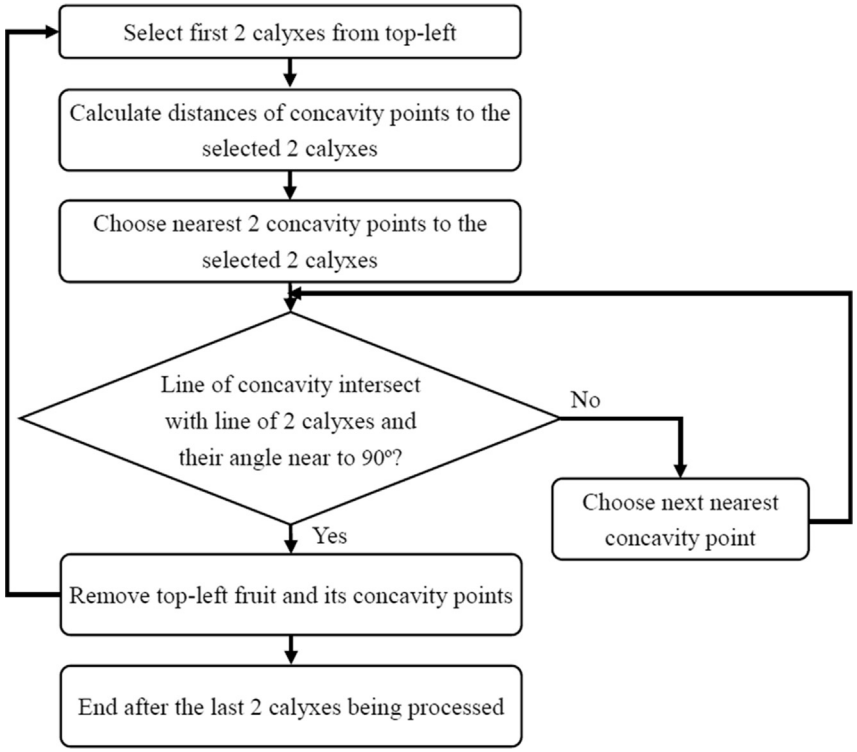

Fig. 6 – Flow chart of the work sequence of the proposed method to separate kiwifruits based on the detected calyxes and concavity points.

and Blue channels are widely distributed, covering almost the entire range caused by the varied illuminations of the daytime and night time during image capturing. The results also revealed that the distribution of the Saturation and Value channels changed sharply and, therefore, it is difficult to utilise them for the segmentation between the skin and calyx. On the other hand, the distribution of the Hue channel was relatively concentrated and stable, and there was less overlap between the distributions of the skin and calyx compared to the Green and Blue channels.

The first two PCs accounted for 72% (PC1) and 26% (PC2) were sufficient to explain a variance of more than 95% for the classification between the skin and calyx pixels (Table 2). The Hue channel exhibited the highest correlation coefficient

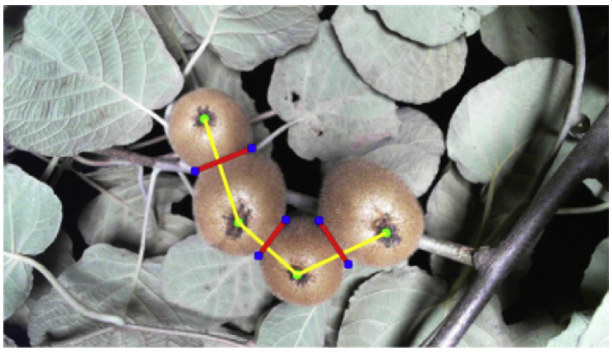

Fig. 7 – Results of applying the fruit separation method to the algorithm, where the green dots are the detected calyxes, the blue square dots are the detected concavity points, the yellow lines are connections between two adjacent fruits and the red lines are the detected splitting paths for separating fruits.

(0.99), and the Red channel recorded the second highest absolute value for the PC1. However, the Red channel showed the highest correlation coefficient (0.62) for the PC2. Therefore, the Hue and Red channels were selected to apply the linear discriminant analysis to segment the pixels of the skin and calyx. The success rates of the sampled pixels were 84.8% for skin, 88.0% for calyx and 86.4% in total. Although these results are not very high, they were acceptable for images under varied lighting conditions.

3.2. *Detection of calyxes*

Table 3 shows the number of calyxes detected in accordance with the number of objects in a single cluster for all the validation dataset images of different lighting conditions. The numbers in parentheses show the percentage of the false positive undetected and the true positive detected calyxes in each category and in the total. The undetected calyxes are the target calyxes in the field of view of the camera, but not detected by the algorithm during image processing. On the other hand, the false positive calyxes are those detected during the image processing although they are not calyxes. The true positive calyxes are those detected during the image processing and are actual calyxes.

Table 2 – Correlation coefficients of the principal components (PC1 and PC2) for the classification between the fruit skin and calyx pixels.

Colour channel	PC1 (72%)	PC2 (26%)
Red	−0.10	0.62
Green	−0.04	0.56
Blue	0.04	0.50
Hue	0.99	0.07
Saturation	-5.85×10^{-4}	4.6×10^{-4}
Value	5.47×10^{-2}	2.18×10^{-3}

Most of the total examined clusters (90.0%) consist of 2–4 fruits. Only 15 of the total 150 randomly selected clusters (i.e. 10.0%) consist of more than 4 fruits. This is consistent with the field survey which concluded that most of the kiwifruit clusters include 2 to 4 fruits (Fu, Wang, et al., 2015).

The true positive detection rates decreased as the number of fruits increased in a cluster; which were 97.0%, 94.8%, 93.3% and 89.0% for the 2-Fruit, 3-Fruit, 4-Fruit and 4+-Fruit clusters, respectively. Similarly, the number of undetected fruits increased as more fruits were forming the cluster. The undetected fruits increased were 3.0% for the 2-Fruit clusters, 5.2% for the 3-Fruit clusters, 6.7% for the 4-Fruit clusters, and 11.0% for the 4+-Fruit cluster.

The undetected fruits were found mainly in clusters containing 4 or more fruits, where the light intensity within the fruits was generally not uniform, as shown in Fig. 7. The far-left fruit in Fig. 9b has a brighter colour, which induced a

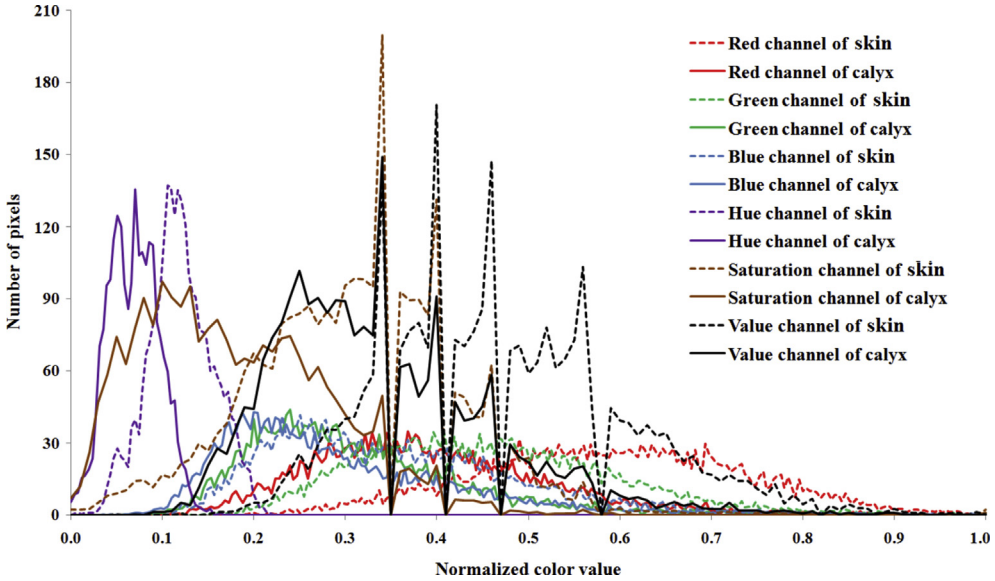

Fig. 8 – Distributions of the Red, Green, Blue, Hue, Saturation, and Value channels of the 5940 skin and calyx pixels sampled from the calibration dataset.

Table 3 – Number of calyxes detected at the different number of fruit objects in the linear cluster.

	4+-Fruit	4-Fruit	3-Fruit	2-Fruit	Total
Number of clusters	15	45	45	45	150
Fruits in all clusters	82	180	135	90	487
Number of images	45	135	135	135	450
Fruits in all images	246	540	405	270	1461
Undetected calyx	27 (11.0%)	36 (6.7%)	21 (5.2%)	8 (3.0%)	92 (6.3%)
False positive calyx	29 (11.8%)	58 (10.7%)	42 (10.4%)	27 (10.0%)	156 (10.7%)
True positive calyx	219 (89.0%)	504 (93.3%)	384 (94.8%)	262 (97.0%)	1369 (93.7%)

Note: Number of images is three times more than clusters as each cluster was imaged at the three lighting conditions. The percentage in brackets is of the total number of calyxes in each category and total.

small area of calyx less than 1/5 of the reference area (Fig. 9a) which was undetected.

There is no significant difference in the false positive detection rate among the different clusters, as shown in Table 3. The false positive detection of calyxes is mostly caused by wrong pixel classification between skin and calyx, resulting in creating more than one black area of one calyx, as shown in Fig. 10a. However, it was improved by calculating the distance l_i (i = 1, 2, …, *fn*-1) between the nearest two detected calyxes and comparing it with the sum *l* of all l_i. If l_i is less than l/2 (*fn*-1), the i^{th} and $(i+1)^{th}$ calyxes can be merged into one calyx by calculating their average position as the new position. The improved results of Fig. 10b are illustrated in Fig. 10c. In total, the false positive detection rate dropped to 5.8%.

The results of the calyx detection in the kiwifruits images captured under different lighting conditions are shown in Fig. 11. The images captured at daytime without flash showed the highest rates of non-detection (9.7%) and false positive detection of fruits (7.6%). On the other hand, the kiwifruit images captured at daytime with flash showed results of approximately 2% better than the images without flash. That was because the images captured without flash had a lower intensity than the images with flash particularly at the fruit contact area, as shown at the red rectangles in Fig. 12a and Fig. 12d. The results were a false positive detection of a black area (Fig. 12b) and a calyx (Fig. 12c) in the images captured without flash. On the other hand, the same cluster image with flash did not have any false positive detection of calyxes, as shown in Fig. 12e and Fig. 12f. The highest true positive detection rate of 98.2% was achieved for kiwifruit images captured at night using the flash, where the flash ensured a constant illumination without influence of sunlight.

3.3. *Separation of kiwifruits*

The results of separating kiwifruits in all images, of the validation dataset, captured under the different lighting conditions are shown in Table 4. The splitting paths are the actual lines (red lines) required to separate all the adjacent kiwifruits in each category. The undetected splitting paths, however, were mainly induced by the undetected calyxes, shown in Fig. 13a, which represented the separation results of Fig. 9b. The results revealed that 8.9%, 10.4%, 11.1% and 14.9% of the actual splitting paths for the 2-Fruit, 3-Fruit, 4-Fruit and 4+-Fruit clusters, respectively, were higher than that for the calyx detection presented in Table 3. However, the false positive detection rates for the four categories of 6.5%, 6.7%, 6.7% and 5.9%, respectively, were lower than that of the calyx detection. That was because the false detected calyxes were mainly at the contact area between kiwifruits. However, they did not affect identifying the splitting path in the developed algorithm, as shown in Fig. 13b. This figure represented the separation results of Fig. 12c, which has a false positive detection of a calyx. There were no differences, however, in the separation results of Fig. 12f, which did not have false positive detection of any calyx, as shown in Fig. 13c. As a result, it is possible to reduce the false positive detection rate of the calyx by connecting their positions, which will be implemented in future research.

The false positive splitting paths were mainly caused by the false positive detection of calyxes, as shown in Fig. 14. Six calyxes were detected in a 4-Fruit cluster under daylight without flash (Fig. 14a), out of which calyxes No. 3 and No. 5, counting from left, were falsely detected. The calyx No. 3 forced the second false positive splitting path, counting from

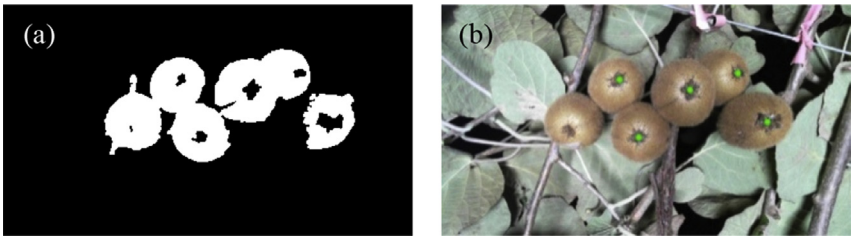

Fig. 9 – An example of undetected calyxes. The leftmost fruit in (b) has a brighter colour, which induces a small area of calyx in (a) that is less than 1/5 of the reference area and is not detected.

Fig. 10 – An example of false positive detection of calyxes (b), which caused by incorrect pixel classification between skin and calyx that resulting in more than one black area of one calyx (a), and its improvement (c) by merging too near calyxes into one calyx.

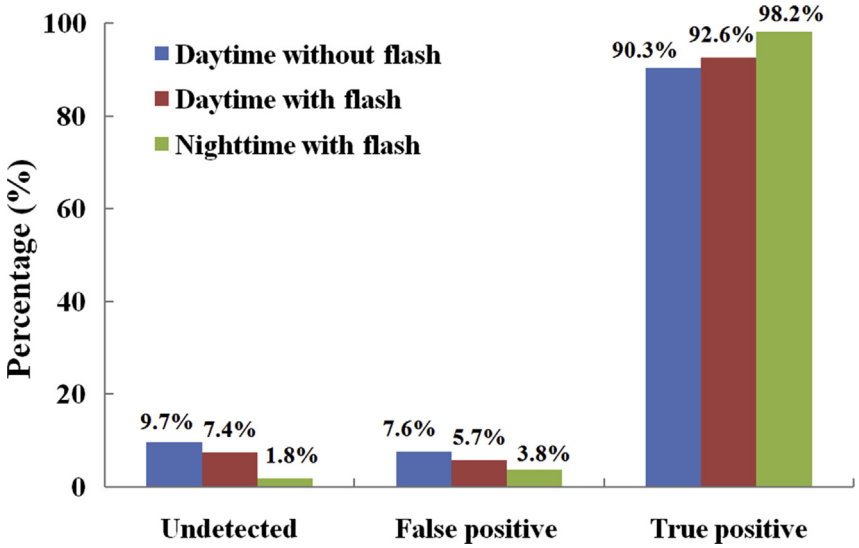

Fig. 11 – Calyxes detection results of kiwifruit images under different lighting conditions.

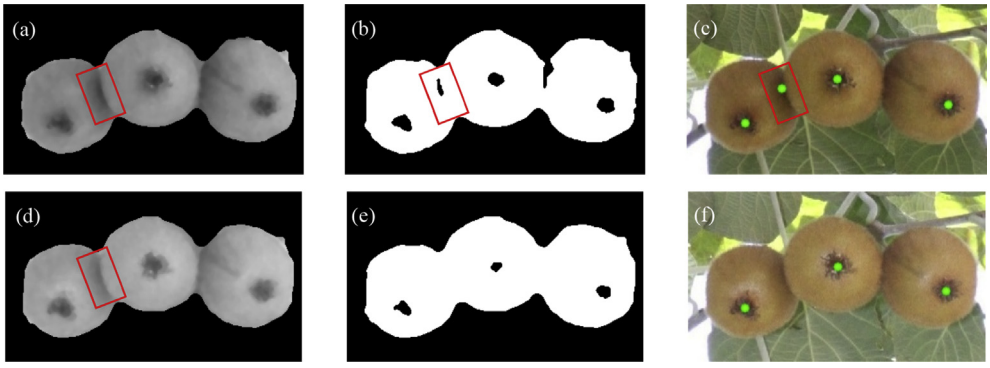

Fig. 12 – Calyx detection results for one cluster of kiwifruits under lighting conditions of daytime without flash (upper row) and with flash (lower row). The original RGB images are in the third column. The first column represented the extracted grey images of the fruit area. The second column represented the black and white images after segmentation between the fruit and calyx. The third column represented the detected calyxes on the original RGB images.

Table 4 – Number of splitting paths detected at the different number of fruit objects in the cluster.

	4+-Fruit cluster	4-Fruit cluster	3-Fruit cluster	2-Fruit cluster	Total
Actual splitting paths	201	405	270	135	1011
Undetected paths	30 (14.9%)	45 (11.1%)	28 (10.4%)	12 (8.9%)	115 (11.4%)
False positive paths	13 (6.5%)	27 (6.7%)	18 (6.7%)	8 (5.9%)	66 (6.5%)
True positive paths	171 (85.1%)	360 (88.9%)	242 (89.6%)	123 (91.1%)	896 (88.6%)

Note: Percentage in () is of the total number of splitting paths in each category and of the total.

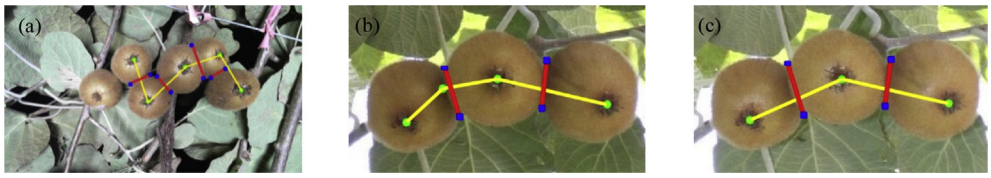

Fig. 13 – Separation results of (a) Fig. 9b, (b) Fig. 12c and (c) Fig. 12f.

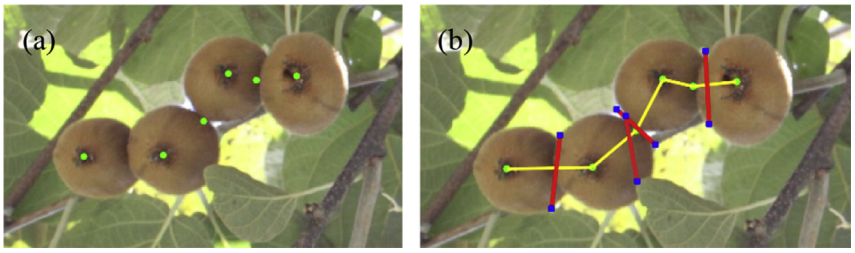

Fig. 14 – Examples of false positive detection of splitting paths (b) of a 4-Fruit cluster with 6 detected calyxes (a) under daylight without flash.

left, as shown in Fig. 14b. On the other hand, the fifth calyx didn't cause a false positive detection of splitting path because there was no concavity point to construct a splitting path, which is also observed in Fig. 13b. For the same reason, it was possible to reduce the false positive rate of the splitting path detection by connecting their positions with that of the detected calyxes, and this will be implemented in future research.

The detection results of the splitting paths of kiwifruit images captured under different lighting conditions are presented in Fig. 15. Kiwifruit images captured at daytime without flash showed the highest rates of non-detection, and false positive fruits detection of 14.2% and 7.4%, respectively. On the other hand, kiwifruit images captured at daytime with flash exhibited better results of 11.9% and 6.5%, respectively. The highest true positive detection rate of 92.0% was observed on the kiwifruit images captured at night time with flash. It was found that the differences among the false positive detection rates of the splitting paths under the three lighting conditions were smaller than that of the calyx. This is attributed to the small effect of the false positive detection of calyxes on the detection of the splitting paths.

In total, 896 splitting paths (88.6%) were correctly detected. The proposed machine vision algorithm took 1.21 s, on average, to process an image, out of which 0.72 s spent on the fruit area segmentation and 0.49 s on the calyx detection and fruit separation. For each fruit, 0.33 s is needed for the detection and separation. It is faster than the algorithm developed by Fu & Wang et al. (2015) which employed a minimal bounding rectangle and an elliptical Hough transform to detect each target fruit area (0.83 s to segment the fruit area and 1.51 s to recognise each fruit on an average) using MATLAB on the same laptop. The algorithms were non-compiled and written in MATLAB and included drawing analysis information to the screen. MATLAB has some advantages as a development environment but not suitable for end application. Significant performance increase will be gained from translating the developed algorithms into a more

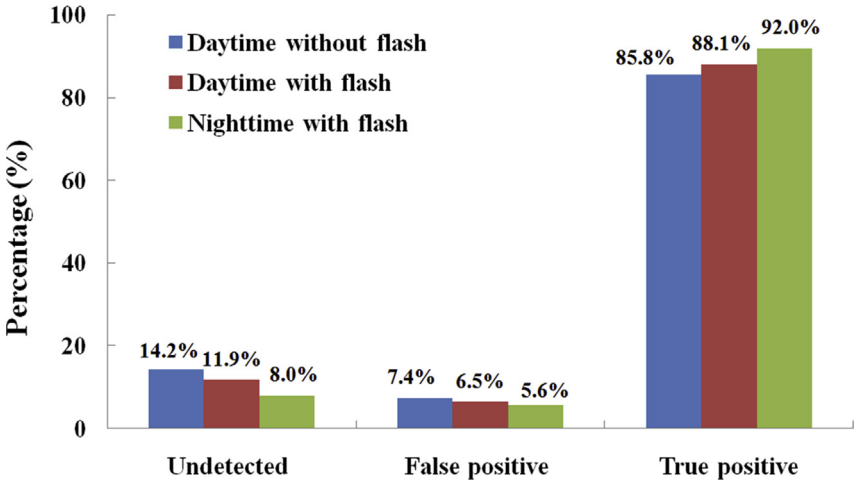

Fig. 15 – Separation results of kiwifruit images captured under different lighting conditions.

suitable language (one of the C family of languages) with OpenCV (Matuska, Hudec, & Benco, 2012, pp. 75–78). On the other hand, state-of-the-art approaches of deep convolutional neural networks have been employed to detect fruits in field, such as apples (Chen et al., 2017), kiwifruits (Fu et al., 2018), and passion fruits (Tu et al., 2018). Although these methods are showing high detection accuracy of fruits with promising processing time on powerful computers with GPUs, their abilities to perform efficiently under field conditions with portable devices with GPUs need to be verified.

4. Conclusions

An algorithm was developed to detect the fruits one by one when they were clustered in-line. Fruits were first segmented from the background, which included the sky, leaves, branches and twigs. Then the fruits calyx was distinguished from the skin, based on colour differences. Next, a calyx line was drawn to connect all calyxes in a single cluster together from the left-top to the right-bottom. Then, the periphery of the cluster was scanned to determine the contact points between the adjacent fruits. Finally, a separating line was drawn between the two closest contact points, provided that this line intersects vertically with the calyx line. In night time with flash, 92.0% of the fruits were separated and counted accurately by the algorithm. Since most of the fruits on the plant are clustered in-line, this algorithm will help in speeding up the harvesting process once implemented in the machine vision system that controls a kiwifruit-picking robotic end-effector. There were two reasons found for the unsuccessful detection. The first was the failure of the algorithm in distinguishing calyxes either by overlooking some of the actual calyxes or by distinguishing noise as calyx. The second was the failure in distinguishing some of the contact points due to the rough periphery of the cluster. Both reasons were found to be related to the original segmentation method of separating the fruits from the background. The ability to overcome these two problems may improve the results under different lighting conditions.

Funding

This work was supported by the Key Research and Development Program in Shaanxi Province of China (grant number 2018TSCXL-NY-05-04, 2017NY-164), and the International Scientific and Technological Cooperation Foundation of Northwest A&F University (grant number A213021505).

Acknowledgements

The authors would like to express their gratitude to the "Young Faculty Study Abroad Program" of the Northwest A&F University Scholarship who sponsored Dr. Longsheng Fu in conducting post-doctoral research at the Centre for Precision and Automated Agricultural Systems, Washington State University. They extend gratitude to the Mexian Kiwifruit Experimentation Station of Northwest A&F University who provided the experimental field.

REFERENCES

Bechar, A., & Vigneault, C. (2016). Agricultural robots for field operations: Concepts and components. *Biosystems Engineering, 149*, 94–111. https://doi.org/10.1016/j.biosystemseng.2016.06.014.

Chaves-González, J. M., Vega-Rodríguez, M. A., Gómez-Pulido, J. A., & Sánchez-Pérez, J. M. (2010). Detecting skin in face recognition systems: A colour spaces study. *Digital Signal Processing, 20*(3), 806–823. https://doi.org/10.1016/j.dsp.2009.10.008.

Chen, S., Shivakumar, S., Dcunha, S., Das, J., Okon, E., Qu, C., et al. (2017). Counting apples and oranges with deep learning: A data-driven approach. *IEEE Robotics and Automation Letters, 2*(2), 781–788. https://doi.org/10.1109/LRA.2017.2651944.

Cui, Y., Su, S., Wang, X., Tian, Y., Li, P., & Zhang, F. (2013). Recognition and feature extraction of kiwifruit in natural environment based on machine vision. *Transactions of the Chinese Society of Agricultural Machinery, 44*(5), 247–252. https://doi.org/10.6041/j.issn.1000-1298.2013.05.043 (in Chinese with English abstract).

Fu, L., Feng, Y., Majeed, Y., Zhang, X., Zhang, J., Karkee, M., et al. (2018). Kiwifruit detection in field images using Faster R-CNN with ZFNet. *IFAC Papers Online, 51*(17), 45–50. https://doi.org/10.1016/j.ifacol.2018.08.059.

Fu, L., Sun, S., Li, R., & Wang, S. (2016). Classification of kiwifruit grades based on fruit shape using a single camera. *Sensors, 16*(7), 1012. https://doi.org/10.3390/s16071012.

Fu, L., Sun, S., Manuel, V.-A., Li, S., Li, R., & Cui, Y. (2017). Kiwifruit recognition method at night based on fruit calyx image. *Transactions of the Chinese Society of Agricultural Engineering, 33*(2), 199–204. https://doi.org/10.11975/j.issn.1002-6819.2017.02.027 (in Chinese with English abstract).

Fu, L., Wang, B., Cui, Y., Su, S., Gejima, Y., & Kobayashi, T. (2015a). Kiwifruit recognition at night-time using artificial lighting based on machine vision. *International Journal of Agricultural and Biological Engineering, 8*(4), 52–59. https://doi.org/10.3965/j.ijabe.20150804.1576.

Fu, L., Zhang, F., Gejima, Y., Li, Z., Wang, B., & Cui, Y. (2015b). Development and experiment of end-effector for kiwifruit harvesting robot. *Transactions of the Chinese Society of Agricultural Machinery, 46*(3), 1–8. https://doi.org/10.6041/j.issn.1000-1298.2015.03.001 (in Chinese with English abstract).

Hannan, M. W., Burks, T. F., & Bulanon, D. M. (2009). A machine vision algorithm combining adaptive segmentation and shape analysis for orange fruit detection. *Agricultural Engineering International CIGR Journal, 11*(1), 1281.

Huang, H., & Ferguson, A. R. (2001). Review: Kiwifruit in China. *New Zealand Journal of Crop and Horticultural Science, 29*(1), 1–14.

Hu, F., Shi, L., Li, R., Li, S., Li, X., Wang, X., et al. (2017). Fertilization evaluation of kiwifruit in Guanzhong region of Shaanxi province. *Soils and Fertilisers Sciences in China,* 54(3), 44–49. https://doi.org/10.11838/sfsc.20170308.

Lu, Y., Chen, Z., Kang, T., Zhang, X., Bellarby, J., & Zhou, J. (2016). Land-use changes from arable crop to kiwi-orchard increased nutrient surpluses and accumulation in soils. *Agriculture Ecosystems and Environment, 223*, 270–277. https://doi.org/10.1016/j.agee.2016.03.019.

Lv, J., Zhao, D., Ji, W., & Ding, S. (2016). Recognition of apple fruit in natural environment. *Optik, 127*(3), 1354–1362. https://doi.org/10.1016/j.ijleo.2015.10.177.

Matuska, S., Hudec, R., & Benco, M. (2012). The comparison of CPU time consumption for image processing algorithm in Matlab

and OpenCV. In *9th international conference on Elektro. Rajecke Teplice, Slovakia, 2012*.

Mebatsion, H. K., & Paliwal, J. (2011). A Fourier analysis based algorithm to separate touching kernels in digital images. *Biosystems Engineering, 108*(1), 66–74. https://doi.org/10.1016/j.biosystemseng.2010.10.011.

Mehta, S. S., & Burks, T. F. (2014). Vision-based control of robotic manipulator for citrus harvesting. *Computers and Electronics in Agriculture, 102*, 146–158. https://doi.org/10.1016/j.compag.2014.01.003.

Mu, L., Liu, H., Cui, Y., Fu, L., & Gejima, Y. (2018). Mechanised technologies for scaffolding cultivation in the kiwifruit industry: A review. *Information Processing in Agriculture*. available online https://doi.org/10.1016/j.inpa.2018.07.005.

Mu, L., Liu, Y., Cui, Y., Liu, H., Chen, L., Fu, L., et al. (2017). Design of end-effector for kiwifruit harvesting robot experiment. In *2017 ASABE Annual International Meeting, Paper No. 1700666, Spokane, USA*. https://doi.org/10.13031/aim.201700666.

Okamoto, H., & Lee, W. S. (2009). Green citrus detection using hyperspectral imaging. *Computers and Electronics in Agriculture, 66*(2), 201–208. https://doi.org/10.1016/j.compag.2009.02.004.

Otsu, N. (1975). A threshold selection method from gray-level histograms. *Automatica, 11*(4), 23–27. https://doi.org/10.1109/TSMC.1979.4310076.

Scarfe, A. J. (2012). *Development of an autonomous kiwifruit harvester: A thesis presented in partial fulfilment of the requirements for the degree of doctor of philosophy in industrial automation at Massey University, Manawatu, New Zealand. EMBARGOED until 15 May 2015*. Massey University.

Scarfe, A. J., Flemmer, R. C., Bakker, H. H., & Flemmer, C. L. (2009). Development of an autonomous kiwifruit picking robot. In *4th international conference on autonomous robots and agents* (pp. 380–384). Wellington, New Zealand: IEEE.

Si, Y., Liu, G., & Feng, J. (2015). Location of apples in trees using stereoscopic vision. *Computers and Electronics in Agriculture, 112*, 68–74. https://doi.org/10.1016/j.compag.2015.01.010.

Silwal, A., Davidson, J. R., Karkee, M., Mo, C. K., Zhang, Q., & Lewis, K. (2017). Design, integration, and field evaluation of a robotic apple harvester. *Journal of Field Robotics, 34*(6), 1140–1159. https://doi.org/10.1002/rob.21715.

Silwal, A., Karkee, M., & Zhang, Q. (2016). A hierarchical approach to apple identification for robotic harvesting. *Transactions of the ASABE, 59*(5), 1079–1086. https://doi.org/10.13031/trans.59.11619.

Sobottka, K., & Pitas, I. (1996). Face localization and facial feature extraction based on shape and color information. In *Proceedings of 3rd IEEE international conference on image processing* (Vol. 3, pp. 483–486). https://doi.org/10.1109/ICIP.1996.560536.

Su, S., Fu, L., Zhang, F., & Cui, Y. (2013). Image acquisition method of kiwifruit picking robot. In *3rd international conference on control, automation and systems engineering* (pp. 9–12). Auckland, New Zealand: Atlantis Press. https://doi.org/10.2991/case-13.2013.3.

Tu, S., Xue, Y., Zheng, C., Qi, Y., Wan, H., & Mao, L. (2018). Detection of passion fruits and maturity classification using red-green-blue depth images. *Biosystems Engineering, 175*, 156–167. https://doi.org/10.1016/j.biosystemseng.2018.09.004.

UN Food & Agriculture Organization. (2018). *Production of kiwi (fruit) by countries*. Retrieved 2018-08-29.

Yamamoto, K., Guo, W., & Ninomiya, S. (2016). Node detection and internode length estimation of tomato seedlings based on image analysis and machine learning. *Sensors, 16*(7), 1044. https://doi.org/10.3390/s16071044.

Zhan, W., He, D., & Shi, S. (2013). Recognition of kiwifruit in field based on Adaboost algorithm. *Transactions of the Chinese Society of Agricultural Engineering, 29*(23), 140–146. https://doi.org/10.3969/j.issn.1002-6819.2013.23.019 (in Chinese with English abstract).

Zhong, Q., Ping, Z., Yao, Q., & Mao, K. (2010). A novel segmentation algorithm for clustered slender-particles. *Computers and Electronics in Agriculture, 69*(2), 118–127.